Scientia Iranica D (2023) 30(3), 1097–1105

SCIENTIA IRANICA

Sharif University of Technology
Scientia Iranica
Transactions D: Computer Science & Engineering and Electrical Engineering
http://scientiairanica.sharif.edu

Sensorless position control of an axial flux-switching permanent-magnet motor based on high-frequency pulsating voltage vector injection

S. Jamali Arand[a] and J. Rahmani Fard[b,*]

a. *Department of Electrical Engineering, Faculty of Engineering, Yasouj University, Yasouj, Iran.*
b. *Department of Electrical Engineering, Pooyesh Institute of Higher Education, Qom, Iran.*

Received 30 December 2020; received in revised form 26 April 2021; accepted 18 October 2021

KEYWORDS
Permanent magnet;
Flux switching motor;
Sensorless;
Signal injection;
Yokeless.

Abstract. Flux-Switching Permanent-Magnet (FSPM) machines are novel brushless machines with magnets in the stator, which have recently undergone intensive research due to their novel features, such as simple and robust rotor, flux focusing effect, sinusoidal phase back-EMF, high torque/power density, and high efficiency. In this paper, a sensorless High-Frequency (HF) sinusoidal signal injection scheme for a novel yokeless and segmented armature axial flux-switching sandwiched permanent-magnet motor (YASA-AFFSSPM) is proposed. Firstly, pulsating voltage injection is investigated in detail. In addition, a simpler method (direct signal process method) for position error signal processing is presented based on pulsating signal injection. The principle and the realization of this method are analyzed in depth. Through experiment, the traditional signal process method and direct signal process method with HF pulsating sinusoidal signal injection are compared to verify the validity of the proposed method.

1. Introduction

Traditional rotor permanent-magnet motors are widely used due to their simple structure, reliable operation, high efficiency, power density, etc. However, since the permanent magnets are located on the rotor, the cooling conditions are poor and the heat dissipation is difficult, leading to irreversible demagnetization of the permanent magnets and affecting the motor operation and power density. Therefore, stator permanent magnet motors, Double Salient Permanent Magnet (DSPM) motors, and Flux Switching Permanent Magnet (FSPM) motors have been extensively studied in recent years [1–4].

The FSPM motor has the advantages of sinusoidal back-EMF, simple and strong rotor structure, high power density, and strong anti-demagnetization ability, making it very suitable for brushless AC (BLAC) transmission systems. Its mathematical model is the same as the rotor permanent-magnet synchronous motor, and the mature vector control and direct torque control technologies can be widely applied to FSPM motors. A high-performance transmission system needs to install a position sensor to measure the real-time rotor position, while the speed control system has high cost, large size, and low reliability, which limit its application range. In order to overcome the defects caused by mechanical position sensors, scholars have carried out a fair body of research on the sensorless position technologies of AC motors [5–16]. Sensorless

*. *Corresponding author.*
E-mail addresses: s.jamali@yu.ac.ir (S. Jamali Arand); Javad.rahmani.fard@gmail.com (J. Rahmani Fard)

doi: 10.24200/sci.2021.57434.5239

technology reduces the size and cost of the motor and improves the reliability of the system. These technologies can be divided into two categories based on both the back EMF [5–7] and the salient pole effect [8–15]. The method based on the back EMF has superior performance at medium and high speeds, but since the magnitude of the back EMF is proportional to the rotation speed, it is not suitable for zero-speed and low-speed operations. The principle of sensorless position technology based on the salient pole effect is to inject a High-Frequency (HF) signal into the motor to track the salient pole of the motor for achieving a position estimation. HF signal injection is divided into rotation signal injection [8–11] and pulse signal injection, which is suitable for zero-speed and low-speed operations [9,12–14].

The traditional HF sinusoidal signal injection method needs to use a low-pass filter to obtain a position error signal, and the use of a low-pass filter causes signal delay, thereby affecting the performance of the control. An HF square wave injection method to achieve sensorless control of AC motors from zero speed to low speed is proposed in [15]. It eliminates the low-pass filter in the process of obtaining the position error signal so that the control performance is improved and the bandwidth of current loop and speed loop is increased.

Although the mathematical model for the 12/10-pole permanent-magnet flux switching motor and the rotor permanent-magnet synchronous motor (BLAC) is the same [1–3], the rotor has a salient pole structure without permanent magnets and windings. An initial position detection and sensorless control of a 6Slotes/4Poles FSPM motor is presented in [16]. However, a 6Slotes/4poles FSPM motor is equivalent to the control of a BLDC motor and its mathematical model is different from that of a BLAC motor.

In [17], Rahmani-Fard and Ardebili proposed a novel yokeless and segmented armature axial FSPM motor (YASA-AFFSSPM), which had dual-rotor/single-stator and showed more desired performance including low cogging torque, large torque/power density, and high efficiency. This paper studies the zero-speed and low-speed operation of a 12Slotes/19Poles YASA-AFFSSPM motor and investigates a sensorless position control method based on HF pulsating sinusoidal signals.

The traditional signal processing method is analyzed and then, a direct signal process method for position error signal processing is studied. In the direct signal processing method, q-axis current signal of the estimated synchronous rotating reference frame is processed through the Band Pass Filter (BPF) directly multiplied by the square wave signal in order to get the position error signal, which can eliminate the low-pass filter for making the signal process simple. Finally, through experiment, the traditional signal process method and the direct signal process method with HF pulsating sinusoidal signal injection are compared to verify the validity of these methods.

2. Configuration and operation principle

Figures 1 and 2 show the configuration and operation principle of the 12Slots/19Poles YASA-AFFSSPM machine, respectively. The design and operation principle are proposed in detail in [17]. The 3-D FEM model of the 12S/19P YASA-AFFSSPM motor is provided in the "ANSYS Maxwell 16" software. The 3D mesh of the 12S/19P YASA-AFFSSPM motor is illustrated in Figure 3. The open-circuit magnetic flux density distribution is shown in Figure 4.

In the synchronous-rotation d–q coordinate system, the voltage equations of the YASA-AFFSSPM are as follows:

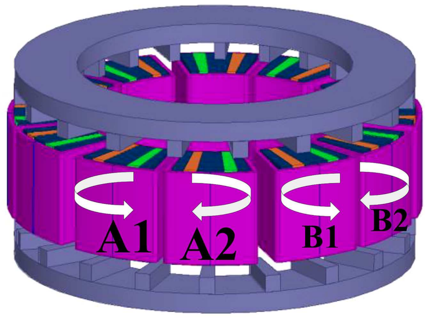

Figure 1. Motor topology.

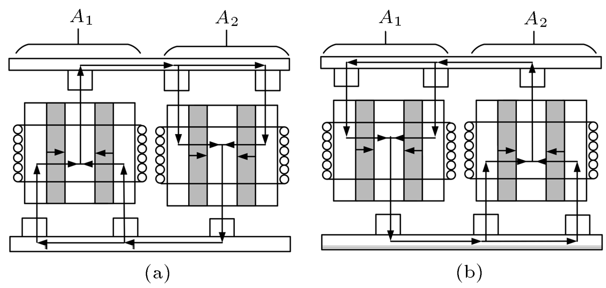

Figure 2. Operation principles: (a) Maximum positive flux linkages and (b) maximum negative flux linkages.

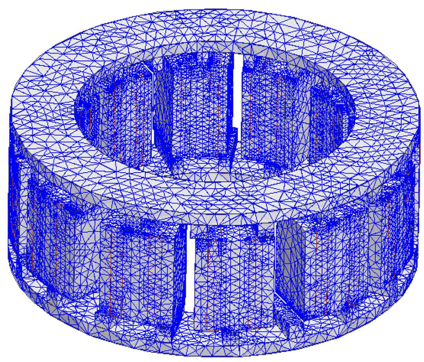

Figure 3. 3-D mesh of the 12S/19P YASA-AFFSSPM motor.

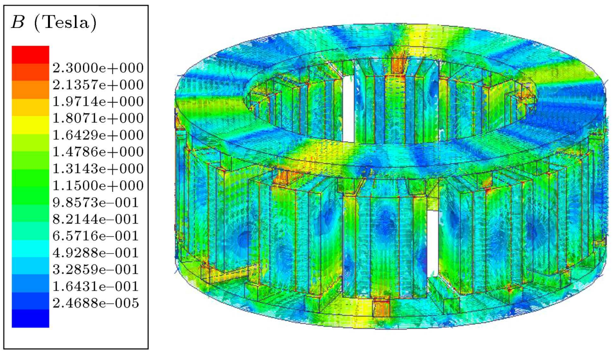

Figure 4. Open-circuit field distribution.

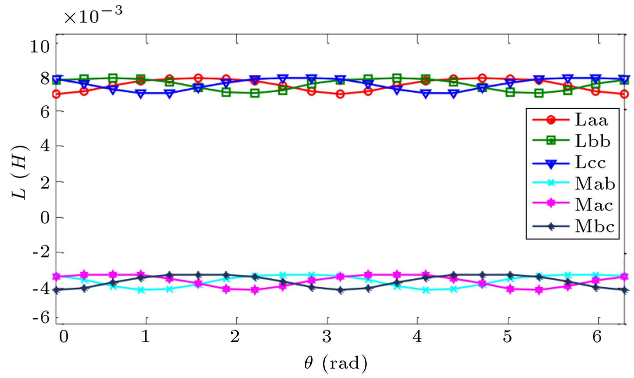

Figure 5. Three-phase self-inductances and mutual inductances.

$$u_d = Ri_d + \frac{d\psi_d}{dt} - \psi_q\omega_e,$$

$$u_q = Ri_d + \frac{d\psi_q}{dt} + \psi_d\omega_e, \tag{1}$$

where u_d and u_q are the dq-axes stator voltages, i_d and i_q are the dq-axes stator currents, ψ_d and ψ_q are the dq-axes stator flux, ω_e is the electrical angular velocity, and R is the armature winding resistance. Moreover, we have $\psi_d = L_d i_d + \psi_m$ and $\psi_q = L_q i_q$, where L_d and L_q are dq-axes inductances and ψ_m is the PM flux linkage. The electromagnetic torque in YASA-AFFSSPM motor can be expressed as:

$$T_{em} = \frac{3}{2}P_r\left(\psi_m I_m \sin\delta - \frac{1}{2}(L_d - L_q)I_m^2 \sin 2\delta\right), \tag{2}$$

where δ is angle torque in the 12/19 YASA-AFFSSPM motor.

Figure 5 shows the three-phase self-inductances and mutual inductances of a 12/19 YASA-AFFSSPM motor obtained by finite element simulation. The inductance changes double in the electric cycle, but the amplitude changes remain small.

Figure 6 shows the calculated d and q axes inductances. It can be seen that the difference between L_d and L_q is small and L_q/L_d is about 1.13. Therefore, the 12/19 YASA-AFFSSPM motor has a salient pole effect ($L_d \neq L_q$). Furthermore, the saliency can be tracked to perform sensorless control of the HF injection method.

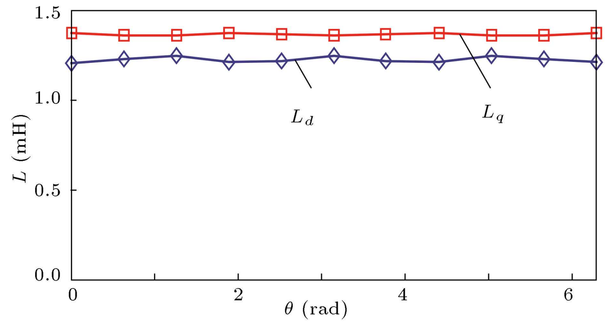

Figure 6. d/q axes inductances.

3. High-Frequency (HF) pulsating sinusoidal signal injection with sensorless control

3.1. The mathematical model of the motor under HF excitation

The HF model of the YASA-AFFSSPM motor in the low-speed condition and at a standstill can be expressed as [18]:

$$\begin{bmatrix} u_d \\ u_q \end{bmatrix} = \begin{bmatrix} j\omega_h L_{dh} + R & 0 \\ 0 & j\omega_h L_{qh} + R \end{bmatrix} \begin{bmatrix} i_d \\ i_q \end{bmatrix}$$

$$= \begin{bmatrix} Z_{dh} & 0 \\ 0 & Z_{qh} \end{bmatrix} \begin{bmatrix} i_d \\ i_q \end{bmatrix}. \tag{3}$$

The HF impedance model, Eq. (3), is used to derive the expression of the induced HF currents for rotor position estimation. The HF pulsating voltage vector is injected into the estimated $\hat{d}\hat{q}$ rotating reference frame. The angle between the $\hat{d}$ axis and the α axis, which is aligned with the direction of the phase A magnetic axis, is defined as the estimated rotor position, as shown in Figure 7. The error between the real θ_{real} and the estimated rotor positions θ_{est} is denoted by $\Delta\theta$, $\Delta\theta = (\theta_{real} - \theta_{est})$.

$$\begin{bmatrix} f_d \\ f_q \end{bmatrix} = \begin{bmatrix} \cos(\Delta\theta) & \sin(\Delta\theta) \\ -\sin(\Delta\theta) & \cos(\Delta\theta) \end{bmatrix} \begin{bmatrix} \hat{f}_d \\ \hat{f}_q \end{bmatrix}. \tag{4}$$

In Eq. (4), f_d and f_q represent the voltage or current in the dq axes coordinate system. According to Eqs. (3) and (4), the mathematical model of the estimated coordinate system is the following:

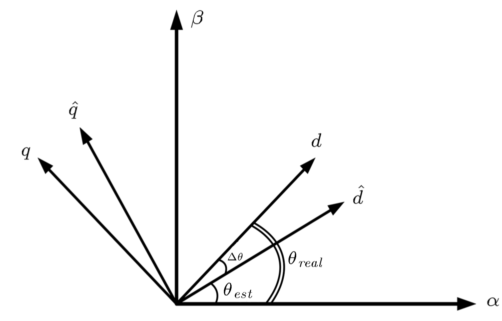

Figure 7. Definition of position error.

$$\begin{bmatrix}\hat{i}_d\\ \hat{i}_q\end{bmatrix}=\frac{1}{Z_{dh}Z_{qh}}\begin{bmatrix}Z-\Delta Z\cos(2\Delta\theta) & -\Delta Z\sin(2\Delta\theta)\\ -\Delta Z\sin(2\Delta\theta) & Z+\Delta Z\cos(2\Delta\theta)\end{bmatrix}\begin{bmatrix}\hat{u}_d\\ \hat{u}_q\end{bmatrix}, \tag{5}$$

where Z and ΔZ can be expressed as:

$$Z=\frac{Z_{dh}+Z_{qh}}{2}, \qquad \Delta Z=\frac{Z_{dh}-Z_{qh}}{2}. \tag{6}$$

3.2. Pulsating voltage injection method and position error signal extraction

An HF sinusoidal voltage vector, described by Eq. (7), is injected into the estimated $\hat{d}\hat{q}$ reference frame [19].

$$\begin{bmatrix}\hat{u}_d\\ \hat{u}_q\end{bmatrix}=\begin{bmatrix}U\cos\omega_h t\\ 0\end{bmatrix}. \tag{7}$$

In the conventional method, the rotor position information is extracted from the induced HF current signals in the $\hat{d}\hat{q}$ reference and from Eq. (5), $\hat{i}_d$ and $\hat{i}_q$ can be expressed as [20]:

$$\hat{i}_d=\frac{Z-\Delta Z\cos(2\Delta\theta)}{Z_{dh}Z_{qh}}U\cos\omega_h t, \tag{8}$$

$$\hat{i}_q=\frac{-\Delta Z\sin(2\Delta\theta)}{Z_{dh}Z_{qh}}U\cos\omega_h t. \tag{9}$$

As shown in Eqs. (8) and (9), the rotor position estimation error, $\Delta\theta$, is contained in $\hat{i}_q$. However, the magnitude of $\hat{i}_q$ depends on the rotor saliency, which is small for a 12S/19P YASA-AFFSSPM. The conventional signal processing method is shown in Figure 6. $\hat{i}_q$ passes through a BPF and then, is multiplied by $\sin(\omega_h t)$. The error signal $f(\Delta\theta)$ is obtained by passing a low-pass filter:

$$f(\Delta\theta)=LFP\left(\hat{i}_q\times\sin(\omega_h t)\right)\approx\frac{(L_q-L_d)}{\omega_h L_q L_d}U\Delta\theta = K\Delta\theta. \tag{10}$$

Therefore, the general transfer function of the position estimation system can be obtained according to Figure 8. Eqs. (11) and (12) are derived from Figure 8 as:

$$\theta_{est}=K\Delta\theta\times\left(K_p+\frac{K_i}{s}\right)\times\frac{1}{s}, \tag{11}$$

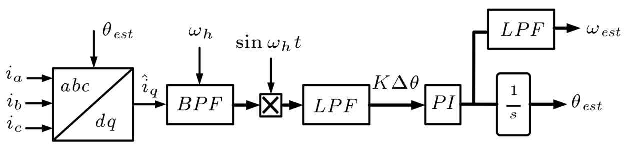

Figure 8. Block diagram of rotor speed estimation by pulsating voltage injection method.

and:

$$\frac{\theta_{est}}{\theta_{real}}=\frac{KK_p s+KK_i}{s^2+KK_p s+KK_i}. \tag{12}$$

From Eq. (12), since $K>0$ and the PI parameters are greater than zero, the poles of the transfer function are located on the left half of the s plane and the steady-state gain of the transfer function is 1. Therefore, the estimated position can track the actual position.

Through analysis, it can be seen that the principle of sensorless control based on the traditional signal processing method is simple, but the process of obtaining the position error signal includes a low-pass filter. The selection of the cut-off frequency affects the performance of the sensorless control. The lower selected the cut-off frequency of the low-pass filter, the larger the position estimation delay of the system will be and on the other hand, the higher the cut-off frequency, the weaker the filter interference signals. Therefore, it is necessary to repeatedly select the cut-off frequency in the actual experiment in order to achieve the best control effect. Based on HF pulsating sinusoidal signal injection, this paper studies a direct signal processing method that can eliminate low-pass filtering and simplify the signal processing process.

4. Direct signal processing method

In the proposed method, the estimated q-axis current, $\hat{i}_q$, can be further simplified to obtain:

$$\hat{i}_q=\frac{j\omega_h(L_d-L_q)\sin(2\Delta\theta)}{2(j\omega_h L_d+R)(j\omega_h L_q+R)}U\cos\omega_h t. \tag{13}$$

By ignoring the resistance, when the HF signal is injected, $\hat{i}_q$ can be reduced as:

$$\hat{i}_q=\frac{(L_d-L_q)\sin\omega_h t}{2\omega_h L_d L_q}U\sin(2\Delta\theta)=K\sin(2\Delta\theta), \tag{14}$$

where:

$$K=\frac{(L_d-L_q)}{2\omega_h L_d L_q}U\sin\omega_h t. \tag{15}$$

Figure 9 shows the relationship between the sine injection signal and the coefficient K. It can be seen that K is a sine function and changes at the frequency ω_h. The traditional signal processing method is to obtain the position error signal by multiplying the sine signal of the same frequency, then low-pass filtering it, and finally entering the position estimation observer.

In the direct signal processing method, the signal $\hat{i}_q$ of the estimated synchronous rotating reference frame is processed through the BPF directly multiplied by the square wave signal to get the position error signal. Therefore, the position error signal $g(\Delta\theta)$ is obtained as follows:

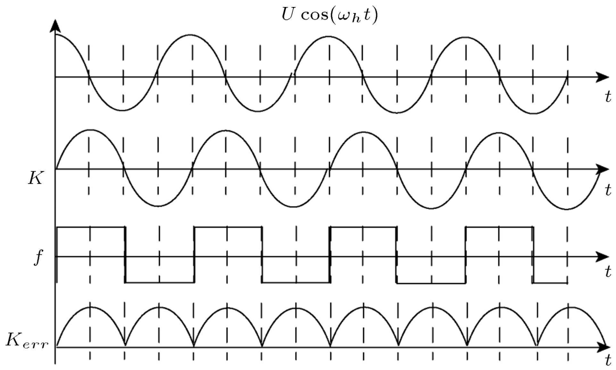

Figure 9. Relations of injected sinusoidal wave signals.

$$g(\Delta\theta) = K\sin(2\Delta\theta) \times f = |K| \times \sin(2\Delta\theta)$$

$$= \frac{(L_q - L_d)}{2\omega_h L_d L_q U}|\sin(\omega_h t)|\sin(2\Delta\theta)$$

$$\approx K_{err}\Delta\theta, \tag{16}$$

where f is the sign function. The signal $g(\Delta\theta)$ is the input to the PI regulator and can be written as:

$$g(\Delta\theta) \times \left(K_p + \frac{K_i}{s}\right) \times \frac{1}{s} \approx K_{err}\Delta\theta \times \left(K_p + \frac{K_i}{s}\right)$$

$$\times \frac{1}{s} = \left(K'_p + \frac{K'_i}{s}\right) \times \frac{1}{s} \times \Delta\theta. \tag{17}$$

As can be seen from Eq. (17), the estimated position depends on the PI parameters. In order to investigate the stability of the position estimation system, the Nyquist criterion is used. The system transfer function is described as:

$$\frac{\theta_{est}}{\theta_{real}} = \frac{K'_p s + K'_i}{s^2 + K'_p s + K'_i}. \tag{18}$$

Since the parameters K'_p and K'_i are time-varying variables, the above equation cannot be solved directly. Hence, it should be transformed into a steady-state space system. Let the intermediate variable be x. Thus, one can write:

$$\dot{x} = Ax + B\theta_{real},$$

$$\theta_{est} = Cx + D\theta_{real}. \tag{19}$$

Using the knowledge of the principle of automatic control, Eq. (19) can be written as:

$$\begin{bmatrix}\dot{x}_1\\ \dot{x}_2\end{bmatrix} = \begin{bmatrix}0 & 1\\ -K'_i & -K'_p\end{bmatrix}\begin{bmatrix}x_1\\ x_2\end{bmatrix} + \begin{bmatrix}K'_p\\ K'_i - (K'_p)^2\end{bmatrix}\theta_{real},$$

$$\theta_{est} = \begin{bmatrix}1 & 0\end{bmatrix}\begin{bmatrix}x_1\\ x_2\end{bmatrix}. \tag{20}$$

The Nyquist curves of the system are obtained using the MATLAB software. As shown in Figure 10, K'_p and K'_i have sinusoidal changes with frequency 500 Hz. According to the Nyquist criterion, every curve versus time is stable, hence the stability of the method is verified and it is clear that the steady-state gain is 1. Thus, the estimated position at steady state is consistent with the actual position. The direct signal processing method is shown in Figure 11, which eliminates the need for the low-pass filter. The overall principle of the HF voltage injection method based on the direct signal processing method is shown in Figure 12.

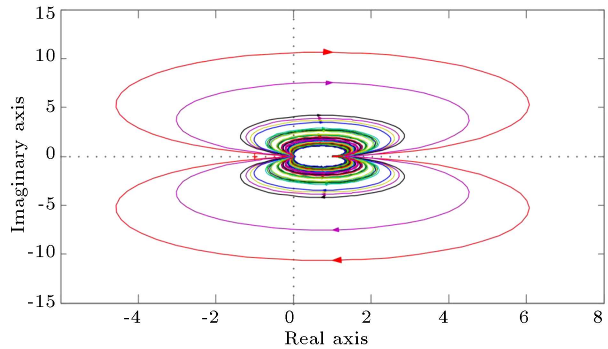

Figure 10. The Nyquist curves.

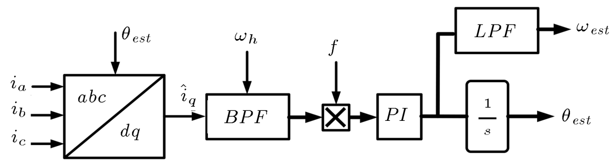

Figure 11. Block diagram of rotor speed/position estimation by the direct signal processing method.

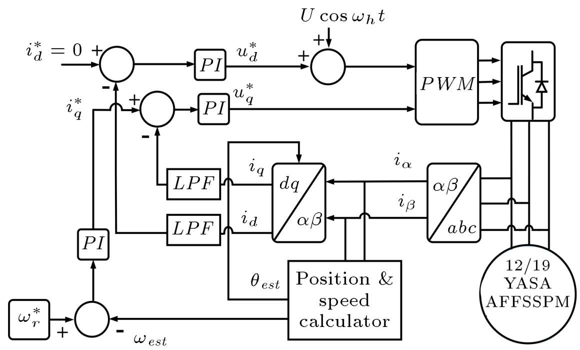

Figure 12. The overall block diagram of a rotating HF sinusoidal injection method.

5. Experimental results

Using the digital control system with TMS320F2812 as the core, the HF pulsating signal injection method is verified by experiment without sensorless control in a 12S/19P YASA-AFFSSPM motor. The switching frequency of the power device is 16 kHz, the amplitude of the injected sine wave voltage signal is 30 V, and the frequency is 500 Hz. The experimental setup is shown

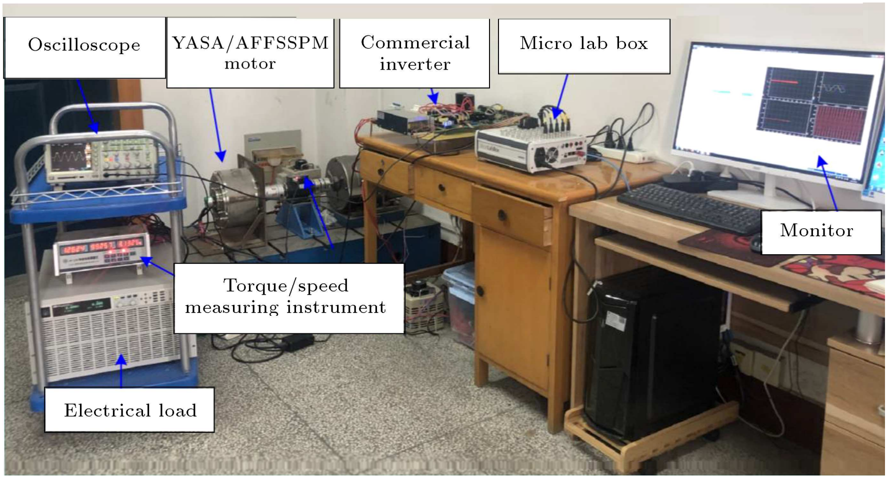

Figure 13. Experimental platform of 12S/19P YASA-AFFSSPM motor.

Table 1. Parameters of 12S/19P YASA-AFFSSPM motor.

Parameter	Value
Rated speed n (rpm)	200
Rated Torque T_n (N.m)	12
Rated Power P (kW)	0.75
PM flux linkage φ_m (Wb)	0.10
Stator resistance R (Ω)	0.65
dq axes rated current $I_d = I_q$ (A)	10
Sampling time T (s)	10^{-4}

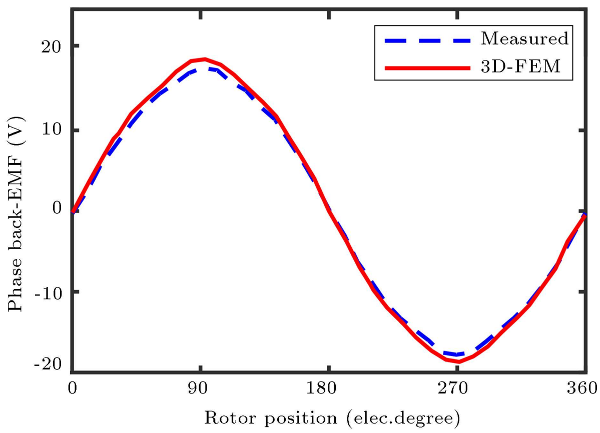

Figure 14. Back-EMF harmonics at 200 r/min.

in Figure 13. Parameters of the investigated motor are shown in Table 1. The back-EMF is shown in Figure 14.

Due to consistency and complementarity of the windings, the back-EMF is highly sinusoidal. In order to verify the sensorless control analysis based on the two signal processing methods, verification experiment of the position error signal is first carried out.

Figure 15(a) shows the position error signal obtained by the traditional low-pass filtering method.

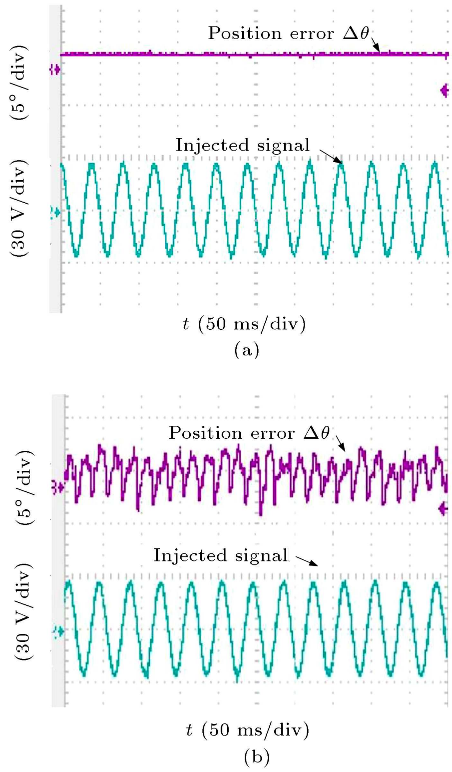

Figure 15. (a) The position error signal obtained by the traditional low-pass filtering method, (b) The position error signal obtained by the direct signal processing method.

The cut-off frequency of the low-pass filter is 5 Hz. Figure 15(b) shows the position error signal obtained by the direct signal processing method. It can be seen that the position error signal changes as an absolute sine wave, which is consistent with Eq. (14).

Figure 16(a) and (b) show the low-speed and sensorless control of two signal processing methods. The position tracking waveforms are given during deceleration from +50 to −50 rpm. Figure 16(a) demonstrates the traditional signal processing method

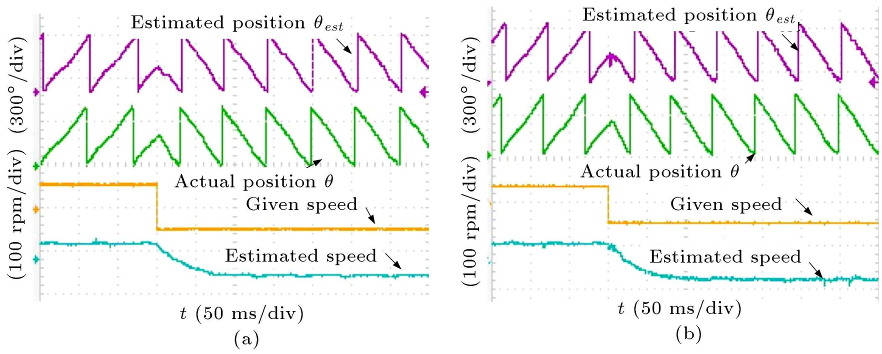

Figure 16. (a) The traditional signal processing method. (b) The direct signal processing method.

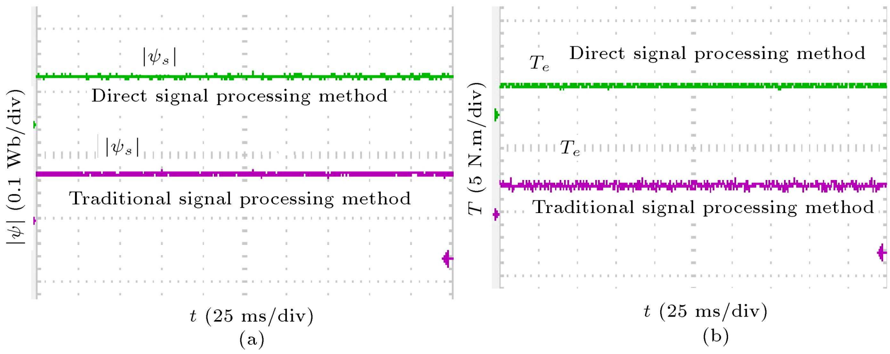

Figure 17. (a) Magnetic flux. (b) Electromagnetic torque.

Table 2. Comparison of the results.

Parameter	Traditional signal processing method (cut-off frequency 5 Hz)	Traditional signal processing method (cut-off frequency 20 HZ)	Direct signal processing method
Flux linkage ripple	4.6%	4.5%	3%
Torque ripple	7%	7%	2.8%
Estimated speed settling time	40 ms	250 ms	39 ms
The ratio of overshoot	30%	0%	0%
Position tracking time	30 ms	230 ms	28 ms

and Figure 16(b) illustrates the direct signal processing method. Both methods can achieve good results without a position sensor. In order to verify the superiority of the direct signal processing method, the difference between the two positions is compared by tracking the initial position of the rotor. The tracking of the position in the two methods is not meaningfully different.

Figure 17 shows the magnetic flux and electromagnetic torque. It can be seen that the flux and torque ripple in the direct signal processing method are lower than those in the traditional signal processing method.

Figure 18 shows the initial position tracking with the two methods. The initial rotor position is 55°. Figure 18(a) and (b) are related to the traditional signal processing method. The low-pass cut-off frequencies are 20 Hz and 5 Hz, respectively. It can be seen that the tracking times are 30 ms and 250 ms. Figure 18(c) is related to the direct signal processing method and the tracking time is 28 ms. The selection of the low-pass filter frequency affects the actual position estimation. Otherwise, a delay occurs in the system. The direct signal processing method tackles the need for low-pass filtering, which makes the signal processing simpler and more effective. For better comparison, the results are listed in Table 2.

6. Conclusion

In this paper, through the finite element analysis and verification of the saliency of the 12/19 poles YASA-AFFSSPM motor, the sensorless position control based on High-Frequency (HF) pulsating sinusoidal signal

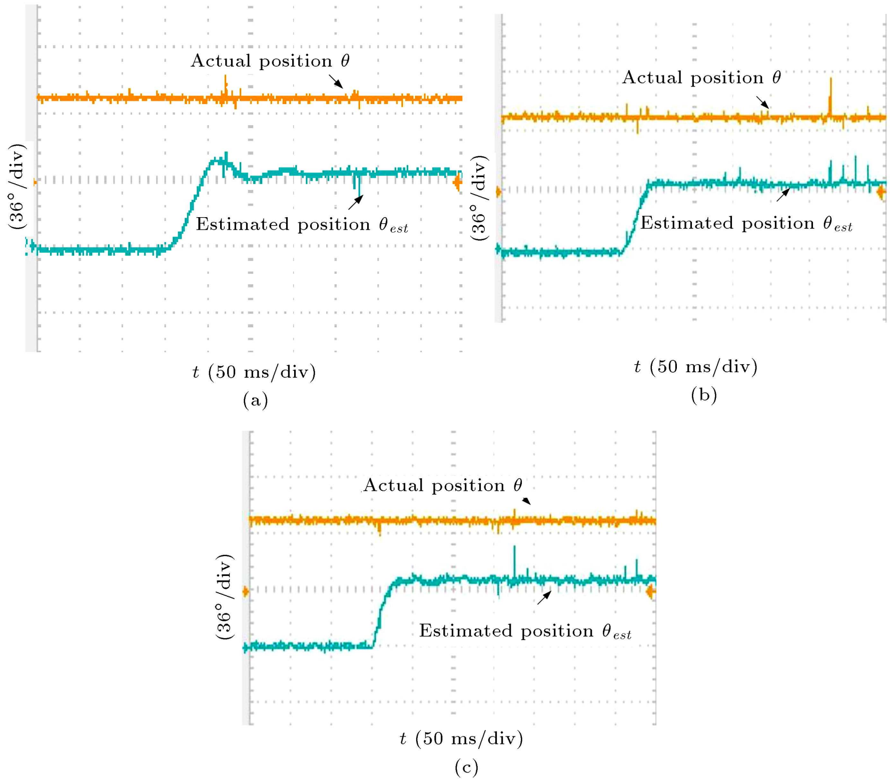

Figure 18. Initial position tracking; (a) Traditional signal processing method with 20 Hz of low-pass cut-off frequency, (b) traditional signal processing method with 5 Hz of low-pass cut-off frequency and (c) direct signal processing method.

injection was studied. Traditional signal processing methods use low-pass filters to obtain position error signals and the selection of the cut-off frequency of the low-pass filter is a demanding task. The sensorless control using the direct signal processing method resolved the need for a low-pass filter, hence the control became simple and effective. Through experiments, the zero-speed and low-speed operation performances of the motor based on traditional signal processing and direct signal processing methods were compared to verify the correctness of the theoretical analysis.

References

1. Zhu, L.L., Xu, D., Li, Q., et al. "Analysis and optimization of equivalent magnetic circuit model for a hybrid axial field flux-switching permanent magnet machine", In *21st International Conference on Electrical Machines and Systems (ICEMS)*, pp. 407–412 (2018).
2. Gandhi, A. and Parsa, L. "Double-rotor flux-switching permanent magnet machine with yokeless stator", *IEEE Trans. Energy Convers.*, **31**(4), pp. 1267–1277 (2016).
3. Zhu, X., Zhengming, S., Li, Q., et al. "Design and multi-condition comparison of two outer-rotor flux-switching permanent-magnet motors for in-wheel traction applications", *IEEE Trans. Ind. Electron.*, **64**(8), pp. 6137–6148 (2017).
4. Medjmadj, S., Demba, D., Claude D., et al. "A salient-pole PMSM position and speed estimation at standstill and low speed by a simplified HF injection method", In *IECON 43rd Annual Conference of the IEEE Industrial Electronics Society*, pp. 8317–8322 (2017).
5. Roggia, S., Francesco, C., Chris G., et al. "Axial position estimation of conical shaped motors for aerospace traction applications", *IEEE Trans. Ind. Electron.*, **53**(6), pp. 5405–5414 (2017).
6. Wang, K. and Lufeng, Z. "Integrated design of high speed permanent magnet machines considering sensorless operation", *IEEJ Trans. Electric. and Electro. Eng.*, **13**(8), pp. 1189–1195 (2018).
7. Genduso, F., Miceli, R., Rando, C., et al. "Back EMF sensorless-control algorithm for high-dynamic performance PMSM", *IEEE Trans. Ind. Electron.*, **57**(6), pp. 2092–2100 (2010).
8. Jansen, P. and Lorenz, R. "Transducerless position and velocity estimation in induction and salient AC machines", *IEEE Trans. Ind. Appl.*, **31**(2), pp. 240–247 (1995).
9. Bianchi, N., Bolognami S., Jang J., et al. "Comparison of PM motor structures and sensorless control techniques for zero-speed rotor position detection", *IEEE Trans. Power Electron.*, **22**(6), pp. 2466–2475 (2007).
10. Xu, P. and Ziqiang, Z. "Carrier signal injection-based sensorless control for permanent magnet synchronous

machine drives with tolerance of signal processing delays", *IET Electric Power Appl.*, **11**(6), pp. 1140–1149 (2017).

11. Wu, X., Sheng, H., Ping L., et al. "A reliable initial rotor position estimation method for sensorless control of interior permanent magnet synchronous motors", *Isa Transactions*, **97**, pp. 116–129 (2020).

12. Ilioudis, V.C. "Sensorless control of permanent magnet synchronous machine with magnetic saliency tracking based on voltage signal injection", *Machines*, **8**(1), pp. 1–20 (2020).

13. Yang, S. and Lorenz, R. "Surface permanent-magnet machine self-sensing at zero and low estimation", *IEEE Trans. Ind. Appl.*, **48**(1), pp. 151–160 (2012).

14. Xing, Z., Li, H., Yang, S., et al. "Improved initial rotor position estimation for PMSM drives based on HF pulsating voltage signal injection", *IEEE Transactions on Industrial Electronics*, **65**(6), pp. 4702–4713 (2017).

15. Bugsch, M. and Piepenbreier, B. "High-bandwidth sensorless control of synchronous reluctance machines in the low-and zero-speed range", *IEEE Trans. Ind. Electron.*, **56**(3), pp. 2663–2672 (2020).

16. Li, C., Gaolin, W., Guoqiang, Z., et al. "Saliency-based sensorless control for SynRM drives with suppression of position estimation error", *IEEE Trans. Ind. Electron.*, **66**(8), pp. 5839–5849 (2018).

17. Rahmani-Fard, J. and Ardebili, M. "Design and control of a novel yokeless axial flux-switching permanent-magnet motor", *IEEE Trans. Energy Convers*, **34**(2), pp. 631–642 (2018).

18. Yao, Y., Huang, Y., Peng, F., et al. "Position sensorless drive and online parameter estimation for surface-mounted pmsms based on adaptive full-state feedback control", *IEEE Trans. Power Electron.*, **35**(7), pp. 7341–7355 (2019).

19. Wang, X., Xie, W., Dajaku, G., et al. "Position self-sensing evaluation of novel CW-IPMSMs with an HF injection method", *IEEE Trans. Ind. Appl.*, **50**(5), pp. 3325–3334 (2014).

20. Siu, M.K.L. and Kam T. Woo. "A high-frequency signal injection based sensorless drive method for brushless DC motor", *18th International Conference on Advanced Robotics (ICAR)*, pp. 367–372 (2017).

Biographies

Saadat Jamali Arand was born in 1981 in Choram, Iran. He received a BSc degree in Electrical Engineering from Isfahan University of Technology (IUT), Iran, in 2003. He also received MSc and PhD degrees in Electrical Power Engineering from K. N. Toosi University of Technology, Tehran, Iran, in 2005 and 2016, respectively. Since 2006, he has been an Instructor of Electrical Engineering at Islamic Azad University, Dehdasht Branch, Iran. Currently, he is an Assistant Professor at Yasouj University. His research interests include modelling, analysis and fault diagnosis of power transformers and electrical machines, power electronics, and renewable energy systems.

Javad Rahmani Fard received the BSc degree from Shahed University, Tehran, Iran, in 2009, and the MS and PhD degrees in Electrical Engineering from K. N. Toosi University of Technology, Tehran, in 2012 and 2018, respectively. Currently, he is an Assistant Professor of Electrical Engineering at Pooyesh Institute of Higher Education, Qom, Iran. His research interests include the analysis and design of electrical machines, sensorless variable-speed drives, and multi-phase variable-speed drives.